Nanoscale

PAPER

View Article Online
View Journal | View Issue

Cite this: *Nanoscale*, 2016, **8**, 1618

Exciton–exciton annihilation and relaxation pathways in semiconducting carbon nanotubes

Jevgenij Chmeliov,[a] Jonas Narkeliunas,[a] Matt W. Graham,[b] Graham R. Fleming[c] and Leonas Valkunas*[a,d]

Received 3rd October 2015,
Accepted 5th December 2015

DOI: 10.1039/c5nr06853c

www.rsc.org/nanoscale

We present a thorough analysis of one- and two-color transient absorption measurements performed on single- and double-walled semiconducting carbon nanotubes. By combining the currently existing models describing exciton–exciton annihilation—the coherent and the diffusion-limited ones—we are able to simultaneously reproduce excitation kinetics following both E_{11} and E_{22} pump conditions. Our simulations revealed the fundamental photophysical behavior of one-dimensional coherent excitons and non-trivial excitation relaxation pathways. In particular, we found that after non-linear annihilation a doubly-excited exciton relaxes directly to its E_{11} state bypassing the intermediate E_{22} manifold, so that after excitation resonant with the E_{11} transition, the E_{22} state remains unpopulated. A quantitative explanation for the observed much faster excitation kinetics probed at E_{22} manifold, comparing to those probed at the E_{11} band, is also provided.

1 Introduction

Carbon nanotubes (CNTs) are hollow cylindrical nanostructures composed of single (in single-walled CNTs) or multiple (in multi-walled CNTs) layers of carbon atoms, rolled up into long tubes with typical diameters of several nm and reported lengths up to several cm.[1] Such an unprecedented length-to-diameter aspect ratio makes CNTs a perfect model of one-dimensional (1D) systems and has resulted in a rapidly growing number of studies, both theoretical and experimental. The unique mechanical and electronic properties make them promising candidates for various applications, from simple usage as composite fibers in polymers to the sophisticated electronic devices like photodiodes,[2] field-effect transistors,[3] or even computers.[4] In semiconducting CNTs, optical excitation in the visible and near-infrared spectral regions leads to the formation of stable electron–hole pairs with the mutual Coulomb interaction being enhanced by the 1D nature of the CNT. As determined from the experimental studies[5,6] and *ab initio* calculations,[7,8] the electron–hole binding energy in CNTs typically ranges from 0.3 to 1 eV and is more than an order of magnitude larger compared to that in bulk three-dimensional semiconducting materials. Advances in the methods of optical spectroscopy have revealed the strong effect of the excitonic properties of CNTs on their absorption and luminescence spectra[5,9,10] as well as sub-ps exciton dynamics in semiconducting single-walled CNTs.[6,11–13]

Depending on the experimental conditions and the considered timescale, many processes were reported to have a strong impact on the overall process of relaxation of the generated excitons in semiconducting CNTs, like the formation of free electrons and holes,[14–17] exciton–phonon interactions,[13,18] formation of the trion states,[19–21] or even triplet–triplet annihilation.[22] Meanwhile, other studies have revealed a pronounced influence of nonlinear exciton–exciton annihilation, especially during the first several ps following the initial ultrafast excitation.[6,11–13] This Auger process consists of a two-particle interaction between the excitons in the first excitonic manifold (E_{11}) resulting in a rapid recombination of one exciton, whereas the other is promoted to a doubly-excited state, $E_{nn} \cong 2E_{11}$, in accordance with energy and momentum conservation. The lifetime of this doubly-excited state is extremely short, and due to the pronounced electron–phonon coupling the exciton finally relaxes back to the E_{11} state.

The important characteristic of the exciton–exciton annihilation process is the annihilation rate constant that on a longer timescale was demonstrated to follow a diffusion-limited behavior: $\gamma(t) \propto t^{d/2-1}$, where d is the dimension of the system.[23,24] This type of exciton–exciton annihilation was then successfully applied to describe transient absorption kinetics, measured in the (6,5) single-walled CNTs under E_{11} excitation.[11] On the other hand, femtosecond fluorescence kine-

[a]Department of Theoretical Physics, Faculty of Physics, Vilnius University, Saulėtekio Ave. 9, LT-10222 Vilnius, Lithuania. E-mail: leonas.valkunas@ff.vu.lt
[b]Department of Physics, Oregon State University, 301 Weniger Hall, Corvallis, Oregon 97331, USA
[c]Department of Chemistry, University of California, Berkeley, California 94720, USA
[d]Institute of Physics, Center for Physical Sciences and Technology, Goštauto 11, LT-01108 Vilnius, Lithuania

tics in the same CNT species were readily described only by assuming a diffusion-free regime of exciton–exciton annihilation.[25] Similar results were also obtained from the two-color pump–probe measurements[12,25,26] of CNTs and led to serious inconsistency since a time-independent annihilation rate is known to be appropriate only for extended systems with a dimensionality greater than 2. As a result, stochastic models describing annihilation of coherent excitons were developed[12,25,27,28] and successfully used to describe the experimentally observed excitation decay kinetics. However, final agreement on the nature of exciton–exciton annihilation in CNTs has still not been achieved.

Recently, we investigated excitation dynamics in semiconducting CNTs following excitation of both E_{11} and E_{22} bands.[12] Transient absorption kinetics corresponding to different excitation conditions, obtained in that work, could be readily described in a quantitative manner only when treated separately, yielding intrinsically inconsistent decay rates. However, difficulties were faced when attempting simultaneous description of both kinetics using the same model parameters, especially on the ps timescale. Therefore, transient absorption kinetics following direct excitation of the E_{22} manifold can provide additional information about the specific properties of singlet–singlet annihilation that were overlooked in the previous studies dealing with single E_{11} or E_{22} pumping conditions.[11,29] An example of such additional information is the insight into the pathways of excitation relaxation following exciton–exciton annihilation. Conventional theoretical description of this process presumes exciton relaxation to occur in a consecutive manner, through all the intermediate excitonic manifolds. However, strong experimental evidence for such a successive process has not been reported. Instead, our recent analysis has suggested the branching scheme for the exciton relaxation from the $E_{nn} \cong 2E_{11}$ state, with one pathway involving the intermediate population of the E_{22} manifold, and another pathway exhibiting direct relaxation to the E_{11} exciton state bypassing the E_{22} state.[12] Thus, for a complete understanding of the processes governing exciton–exciton annihilation, additional studies are needed.

In the current work, we further developed the conventional model of exciton–exciton annihilation by considering both the coherent and the diffusion-limited regimes. The resulting model is applied to our previously measured excitation kinetics in the (6,5) single-walled CNTs as well as the (7,5) inner tube of a double-walled carbon nanotube species[12] and demonstrates good agreement for all excitation conditions over a time range of several fs up to tens of ps. A quantitative explanation for the observed much faster excitation kinetics probed at the E_{22} manifold, compared to those probed at the E_{11} band, is also provided.

2 Methods

The femtosecond transient absorption measurement on (6,5) single-walled CNTs or the inner-tube of (7,5)/(17,6) double-walled CNTs has been fully described elsewhere.[12] The electronic relaxation dynamics of these chiral-enhanced aqueous suspensions of CNTs were measured both in a 200 μm cell and in a PVP polymer matrix.[30,31] The E_{11} or E_{22} transitions were excited resonantly with 60 or 45 fs laser pulses at a 250 kHz repetition rate, respectively. The probe beam was selected to match the resonant transition with an 8 nm bandwidth section of a white-light supercontinuum. The polarization of the pump beam was set to the magic angle (54.7°) with respect to the probe beam.

3 Model for exciton–exciton annihilation

The exciton–exciton annihilation in CNTs is usually described according to a simple kinetic scheme outlined in Fig. 1a and suitable for extended systems with a large number of initially generated excitons. In terms of this model, the populations of the E_{11}, E_{22}, and $E_{nn} \cong 2E_{11}$ exciton manifolds, denoted as n_1, n_2, and n_n, respectively, obey the following Pauli Master equations:[12]

$$\frac{dn_1}{dt} = G_1(t) \cdot f_1 - \gamma(t) n_1^2 + k_{n1} n_n \cdot f_1 + k_{21} n_2 \cdot f_1 - K n_1, \quad (1)$$

$$\frac{dn_2}{dt} = G_2(t) \cdot f_2 + k_{n2} n_n \cdot f_2 - k_{21} n_2 \cdot f_1, \quad (2)$$

$$\frac{dn_n}{dt} = \frac{1}{2}\gamma(t) n_1^2 - (k_{n1} \cdot f_1 + k_{n2} \cdot f_2) n_n, \quad (3)$$

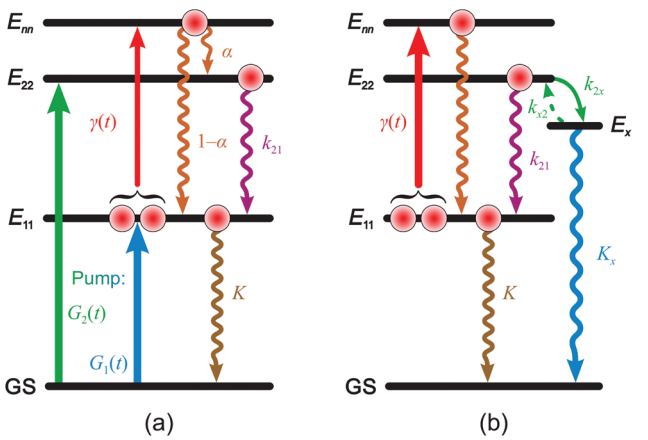

Fig. 1 (a) Schematic energy level diagram that is usually used to describe exciton dynamics in CNTs. Black lines correspond to the excitonic states participating in the exciton–exciton annihilation while arrows indicate possible transitions between these energetic states. Additionally, branching factor α determining relaxation from the doubly-excited state, $E_{nn} \cong 2E_{11}$, is taken into account. (b) Schematic energy level diagram for CNTs that was determined from our modeling of exciton decay kinetics following different excitation conditions at room and 110 K temperatures.

where $G_i(t)$ are the generating functions of the pump pulse corresponding to different excitation conditions (either to the E_{11} or E_{22} state), $\gamma(t)$ is the rate of exciton–exciton annihilation from the E_{11} state, k_{ij} is the linear relaxation rate from the ith to the jth state, and K is the rate of E_{11} exciton decay to the ground state. In order to account for the saturating effect observed at a high excitation density, additional space-filling factors $f_i = 1 - n_i/N_i$ are also considered, here N_i is the maximum number of excitons that can be generated in the ith state.

Since relaxation from the E_{nn} state is usually assumed to be much faster than other typical timescales, eqn (3) can be simplified by assuming a steady-state regime implying $dn_n/dt = 0$, so that

$$n_n \simeq \frac{1}{2}\frac{\gamma(t)}{k_{n1}\cdot f_1 + k_{n2}\cdot f_2}{n_1}^2. \tag{4}$$

If we also define the branching factor of the corresponding relaxation pathway as $\alpha = k_{n2}/(k_{n1} + k_{n2})$, eqn (1) and (2) can be rewritten as follows:

$$\begin{aligned}\frac{dn_1}{dt} &= G_1(t)\cdot f_1 + k_{21}n_2\cdot f_1 - Kn_1 \\ &\quad - \frac{1}{2}\gamma(t){n_1}^2\frac{2\alpha f_2 + (1-\alpha)f_1}{\alpha f_2 + (1-\alpha)f_1},\end{aligned} \tag{5}$$

$$\frac{dn_2}{dt} = G_2(t)\cdot f_2 - k_{21}n_2\cdot f_1 + \frac{1}{2}\gamma(t){n_1}^2\frac{\alpha f_2}{\alpha f_2 + (1-\alpha)f_1}. \tag{6}$$

The transient absorption spectrum $\Delta OD(t,\lambda)$, observed in the pump–probe measurements at different wavelengths λ, is then defined by the exciton populations in various excited states and therefore can be given by[25]

$$\Delta OD(t,\lambda) \propto \sum_i n_i(t)\left[{\sigma_i}^{ESA}(\lambda) - {\sigma_i}^{SE}(\lambda) - \sigma_0(\lambda)\right], \tag{7}$$

where $\sigma_0(\lambda)$ is the ground state absorption spectrum while ${\sigma_i}^{ESA}(\lambda)$ and ${\sigma_i}^{SE}(\lambda)$ are the cross-sections of the excited state absorption and stimulated emission of the ith excited state, respectively. Neglecting the effect of the latter two components and attributing the transient absorption kinetics probed at E_{11} energy merely to the ground state bleaching, we obtain $\Delta OD(t) \propto n_1(t) + n_2(t)$.

The exciton–exciton annihilation rate, $\gamma(t)$, is usually assumed to represent the diffusion-limited excitation relaxation process in an extended system whose size is comparable to or larger than the exciton diffusion radius. For one-dimensional CNTs, the annihilation rate then attains a time-dependent form of $\gamma \propto t^{-1/2}$.[23,24] However, our experimental observations[12] revealed that the transient absorption kinetics possesses the properties of the diffusion-limited regime only asymptotically, with a clear indication of the time-independent annihilation rate on the sub-ps timescale. This result suggests that shortly after the initial excitation, the coherence length of the optically generated excitons is comparable with the nanotube length resulting in coherent exciton annihilation. Later, due to interactions with phonons, the exciton coherence length notably decreases to the typical values of the order of 10 nm as determined from the photoluminescence measurements.[32] As a result, the diffusion-limited annihilation process starts to dominate. The switch from one regime to another occurs gradually; however, there is no theory developed to describe the intermediate process. Therefore, in order to account for both limiting regimes and at the same time not to over-complicate the model, we assume that the time-dependence of the annihilation rate can be approximated by the following simple equation

$$\gamma(t) = \begin{cases} \gamma_0, & \text{for } t \le \tau, \\ \gamma_0\sqrt{\tau/t}, & \text{for } t > \tau, \end{cases} \tag{8}$$

where τ is the mean coherence lifetime, determining the time moment of the switch from coherent exciton–exciton annihilation to the diffusion-limited annihilation. In the second line of eqn (8), an additional factor $\sqrt{\tau}$ ensures the continuity of $\gamma(t)$.

4. Modeling results

4.1 Excitation dynamics in single-walled CNTs at room temperature

The transient absorption kinetics in solubilized (6,5)-enriched single-walled CNTs, measured at room temperature by implementing different resonant excitation wavelengths[12] and E_{11} probe conditions, are presented in Fig. 2a. The multi-exponential behavior of both decay kinetics, normalized at their maximum and corresponding to either E_{11} or E_{22} excitation, clearly indicates the effect of the non-linear annihilation process. Compared to the case of the E_{11} pump conditions, the E_{22} pump excitation kinetics exhibits a considerably slower decay rate on the sub-ps timescale, but both kinetics approach each other at later times and after ~4 ps become indistinguishable. In our previous analysis of these observations,[12] we assumed annihilation of purely coherent excitons and were able to simultaneously describe only the very initial part of both excitation kinetics. However, inclusion of the diffusion-limited part in the annihilation constant in eqn (8) suggests that better results can be obtained on the ps timescale, as proposed in other studies.[11]

The black solid lines in Fig. 2a indicate the best-fitted excitation kinetics assuming purely consecutive excitation decay from the E_{nn} manifold to the E_{11} state *via* the intermediate population of the E_{22} state. Both kinetics were calculated by solving eqn (5) and (6) with the annihilation constant $\gamma(t)$ being expressed by eqn (8) and the generation functions $G_i(t)$ representing the experimental conditions with Gaussian distributions of amplitude $G_{i\max}$ and a full width at half maximum of 60 fs. Similarly to our previous treatment of the initial part of the kinetics,[12] such an assumption of consecutive excitation decay from the E_{nn} manifold cannot provide a reasonable description of both excitation kinetics simultaneously. However, a better result might be expected when the branching scheme illustrated in Fig. 1a is assumed. Such a modifi-

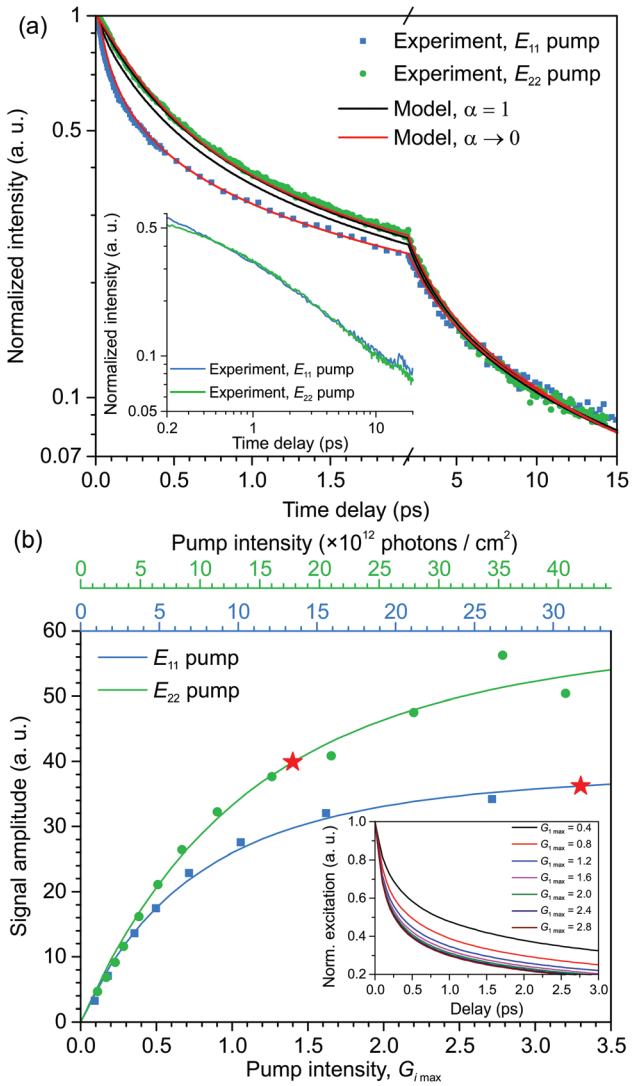

Fig. 2 (a) Normalized transient absorption kinetics probed[12] at the E_{11} manifold in (6,5) CNTs at 292 K (dots) and several best-fitted kinetics simulations calculated according to eqn. (5) and (6) by either fixing the relaxation branching parameter α to 1 (black lines) or allowing it to vary (red lines). Inset: a comparison of both experimental kinetics with that corresponding to the E_{22} pump being shifted to the left by 350 fs along the horizontal axis. (b) Dependence of the calculated maximal ground state bleaching signal, $(n_1(t) + n_2(t))_{max}$, on the excitation intensity G_{imax}, obtained for different pumping conditions using the parameters from Table 1 (lines and bottom axis). Red stars indicate intensities used to obtain excitation kinetics presented in panel (a). For comparison, the corresponding experimental observations[12] are also shown (symbols) by mapping the actually used excitation laser intensities (top axes) to the modeled values of G_{imax}. Inset: normalized excitation kinetics, calculated at different E_{11} pumping amplitudes.

cation to the possible inter-manifold excitation relaxation pathways indeed produced a perfect simultaneous description of both kinetics corresponding to the E_{11} and E_{22} pump conditions, as demonstrated by the red lines in Fig. 2a. Contrary to our previous study,[12] we are now able to reproduce the full experimentally accessible timescale ranging from several fs to 15 ps. Interestingly, during the fitting procedure the branching parameter α eventually converged to zero indicating that upon singlet–singlet annihilation the doubly-excited exciton relaxes directly to the E_{11} state, totally bypassing the intermediate E_{22} manifold. Other obtained model parameters are listed in Table 1.

Table 1 Model parameters used to fit excitation kinetics in Fig. 2a, 3 and 4a

Parameter[a]	(6,5) CNT at 292 K	(6,5) CNT at 110 K	(7,5) inner CNT at 292 K
k_{21}^{-1}	66 fs	63 fs	66 fs
γ_0^{-1}	3.53 ps	3.98 ps	3.95 ps
τ	57 fs	179 fs	48 fs
K^{-1}	52 ps	20 ps	90 ps
$G_{1max}\|N_1$	3.3|40	3.4|37	3.3|36
$G_{2max}\|N_2$	1.4|40	0.7|33	0.5|32
k_{2x}^{-1}	—	0.66 ps	0.14 ps
k_{x2}^{-1}	—	22 ps	17 ps
K_x^{-1}	—	69 ps	21 ps

[a] See Fig. 1 for the notation. Vertical bar in $G_{imax}|N_i$ separates the actual pumping amplitude G_{imax} used to calculate kinetics and the obtained maximum number of allowed excitons in the corresponding state.

Our previous experimental observations[12] revealed that normalized transient absorption kinetics did not exhibit any pronounced dependence on the excitation intensity over a large intensity range. This effect can be understood in terms of the space filling factors $f_i = 1 - n_i/N_i$ (see eqn (5) and (6)) and is further illustrated in the inset of Fig. 2b. Here we see some sensitivity of the normalized decay kinetics to the excitation intensity only for the lowest pumping amplitudes, when merely several excitons per tube are generated. At higher excitation conditions the saturation regime is reached and all the kinetics become indistinguishable, which reflects our experimental conditions. The amplitude of the ground state bleaching signal, $(n_1(t) + n_2(t))_{max}$, also exhibits saturating behavior and is presented with colored lines in Fig. 2b. For comparison, in the same figure we also show the experimentally obtained dependence of the amplitude of the detected signal on the actual pumping intensities[12] that were rescaled to map the maximal values of the generating functions (G_{imax}) used in our simulations. Besides the perfect agreement between our calculated and measured dependencies, it is noteworthy that the ratio of these rescaling factors for the E_{11} and E_{22} pumping conditions (converted from the number of photons to their corresponding energies) is about 0.44, that exactly matches the ratio of the maxima of the E_{11} and E_{22} transitions in the absorption spectrum of (6,5)-tube-enriched aqueous solution.[12] Red stars in Fig. 2b indicate the G_i values that were used to simulate the kinetics shown in Fig. 2a and can be both attributed to approximately the same experimental pumping intensity of ~6 μJ cm^{-2}.

4.2 Excitation dynamics in single-walled CNTs at 110 K

In order to further validate our result of the branching factor $\alpha \approx 0$, we also analyzed excitation dynamics in the same CNT

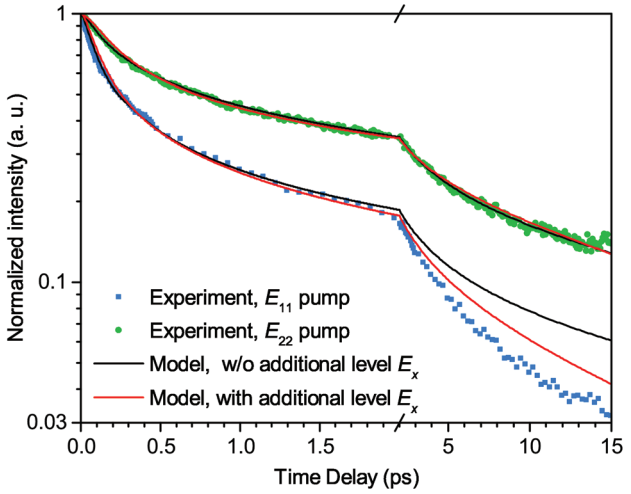

Fig. 3 Normalized transient absorption kinetics, measured in (6,5) CNTs at 110 K under E_{11} and E_{22} excitation conditions (dots).[12] Black lines indicate the best-fitted kinetics corresponding to the ground state bleaching signal and calculated according to eqn (5) and (6); red lines correspond to the case when the additional energy level E_x, shown in Fig. 1b, was accounted for.

species, this time embedded into a polymer film (PVP) and cooled down to 110 K.[12] The corresponding kinetics, probed in the E_{11} manifold, are shown in Fig. 3 and indicate notably different behavior compared to the room temperature data discussed above. The kinetics following E_{22} excitation not only becomes much slower at the initial times, but even asymptotically decays considerably more slowly than in the case of the E_{11} pump (note different asymptotic slopes of both kinetics presented on the semi-logarithmic scale). The later observation cannot be understood in terms of the previously discussed energetic diagram of CNTs (Fig. 1a) since one would expect that, independently of the initial pumping conditions, on the ps timescale all the excitation should reside in the E_{11} state. Due to an asymptotically negligible exciton–exciton annihilation rate, both kinetics should then decay with the same linear rate K, that, however, is not the case. Indeed, the best-fitted kinetics, shown with black lines in Fig. 3a, asymptotically decay in absolutely the same way and do not follow the measured ones. Moreover, for these kinetics the maximal numbers of excitons per manifold, entering the phase-filling factors f_i, were found to differ more than 15 times ($N_1 = 61$ and $N_2 = 4$) that probably do not represent the real situation.

Such a striking asymptotic behavior, however, might be easily understood if one assumes the presence of an additional energy level accessible after the E_{22} excitation and denoted as E_x in Fig. 1b. This state might arise due to interactions with the polymer environment or it can be related to the formation of the exciton surface trap or the generation of a trion state.[20,21] Alternatively, this state can even be one of the optically-dark states belonging intrinsically to CNT itself and predicted by *ab initio* calculations of the excitonic spectra of semiconducting CNTs.[28,33] If the branching factor α is close to 0, the excitation dynamics under E_{11} pump conditions is determined merely by the annihilation rate $\gamma(t)$ and the linear relaxation rate from the E_{11} manifold, K; both E_{22} and E_x states remain unoccupied. However, the overall dynamics can change drastically in the case of direct excitation into the E_{22} manifold. Under such excitation conditions, the E_x state becomes populated and can act as a trap for excitation energy. Provided that both the relaxation rate K_x and the de-trapping rate k_{x2} (see Fig. 1b for the notation) are slower than the linear decay rate K of the E_{11} manifold, the E_{22} state then becomes repopulated at later times resulting in considerably slower excitation dynamics.

The excitation decay kinetics, calculated by assuming this expanded energy level diagram with an additional energy level, is represented by red lines in Fig. 3. Similarly to the case of room temperature measurements, the branching parameter α converged to 0, and the rest of the model parameters used to calculate these kinetics are listed in Table 1. In Fig. 3 we now see a much better agreement with the experimental results as well as the obviously different asymptotic decay rates of the simulated kinetics corresponding to the E_{11} and E_{22} pump conditions. The small discrepancy in the experimental kinetics still appearing after a delay time of $t \geq 5$ ps in the case of E_{11} excitation might indicate the existence of even more additional energy levels, similar in nature with our introduced level E_x. The resulting energy diagram and possible relaxation pathways then become much more complicated.

4.3 Excitation dynamics in double-walled CNTs at room temperature

Similarly to the results shown above, a more complex exciton relaxation scheme might also be expected for the double-walled CNTs due to inter-tube interactions. Indeed, transient absorption measurements of the excitation dynamics in the inner tubes of the (7,5)/(17,6) double-walled CNTs revealed that even at room temperature the two decay kinetics following resonant excitation of the E_{11} and E_{22} transitions did not approach the same asymptotic behavior, at least during the initial several hundreds of ps.[12] In order to quantitatively understand such a striking behavior, we have applied our model to simulate excitation decay kinetics in double-walled CNTs as well.[12] The experimental kinetics together with the best fit are shown in Fig. 4a. Interestingly, for a suitable description of the experimental kinetics we also had to account for the E_x state introduced above. The corresponding fitting parameters are listed in Table 1, and the branching factor α again converged to 0, as we found for single-walled CNTs.

During the experimental measurements it was observed that in the case of E_{22} excitation the amplitude of the detected transient absorption scales linearly with the laser pumping intensity whereas for the E_{11} pump it increases proportionally to the square root of the pumping intensity.[12] These approximately linear dependencies were much more pronounced than in the corresponding measurements of the single-walled CNTs and can be easily reproduced with our model using the same

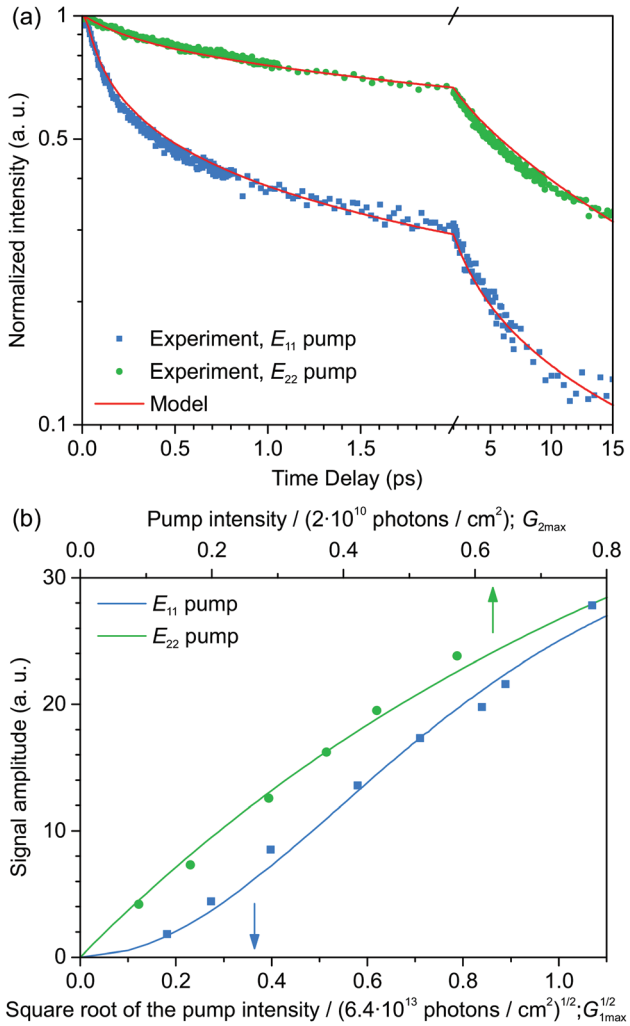

Fig. 4 (a) Normalized transient absorption kinetics, measured for the inner (7,5) tube in double-walled CNTs at 292 K under different excitation conditions[12] (dots) and best-fitted kinetics, calculated assuming the same energy relaxation scheme as in Fig. 1b (red lines). (b) Approximately linear dependence of the calculated maximal ground state bleaching signal on either excitation intensity G_{2max} (E_{22} pump, top axis) or the square root from excitation intensity G_{1max} (E_{11} pump, bottom axis). For comparison, the corresponding experimental observations[12] are also shown with dots by mapping the actual excitation laser intensities to the modeled values of G_{imax}.

parameters obtained from the fitted excitation kinetics, as demonstrated in Fig. 4b. Meanwhile, at higher intensities the effect of the space-filling factors starts to dominate and saturates the intensity curves.

5 Discussion

In previous studies, transient absorption measurements of exciton–exciton annihilation were usually performed by utilizing pump intensities of 10^{14}–10^{16} photons per cm^2.[13,23,25] In our case, however, special care for the sample preparation as well as carefully tuned spectral overlap of the excitation pulse with the E_{11} and E_{22} absorption peaks of the studied CNTs allowed us to generate a similar amount of initial excitons at considerably lower excitation pulse intensities. Indeed, the mean number of the generated excitons can be evaluated as $n_0 \approx \sigma_C N_C I$, where $\sigma_C \approx 10^{-17}$ cm^2 is the mean absorption cross-section of a single carbon atom,[34] $N_C \approx 7.2 \times 10^4$ is the mean number of carbon atoms in our ~800 nm long (6,5) CNTs. For the typical excitation fluence of $I \approx 3 \times 10^{13}$ photons per cm^2 (see red star in Fig. 2b for the E_{11} pump conditions), we obtain $n_0 \approx 22$. This number is very close to the actual number obtained by fitting the corresponding excitation decay kinetics ($n_0 \approx 25$).

By holistically combining the coherent and the diffusion-limited regimes of exciton–exciton annihilation in semiconducting CNTs, we were able to quantitatively reproduce both the E_{11} and E_{22} pump transient absorption kinetics of (6,5) single- and (7,5) double-walled CNT samples for different lattice temperatures. For simplicity, we have not explicitly accounted for the formation of the trions, triplets or exciton–phonon bound states that were previously reported[13,18,19–22] since we did not resolve the distinct temporal and spectral signatures of these quasi-particles during our measurements. Nevertheless, the existence of such additional relaxation pathways might be responsible for the slight mis-fitting of our calculated excitation kinetics, especially in the polymer-composite measurements on the timescale of tens of ps.

The validity of our model was further supported by the calculated intensity dependencies of maximal signal on the excitation amplitude, shown in Fig. 2b and 4b. We found that, at room temperature, the lifetime τ of initially generated coherent excitons in the solubilized CNTs, both single- and double-walled species, is comparable to the duration of the pump pulse. This means that time-independent annihilation of coherent excitons switches to the diffusion-limited regime shortly after the end of the initial excitation, which agrees with the previous studies on excitation-induced dephasing times.[35,36] On the other hand, upon embedding CNTs into a polymer film and cooling them down to 110 K, the coherence lifetime exhibited a 3-fold increase, resulting in more efficient exciton–exciton annihilation and, therefore, faster kinetics under the E_{11} pump conditions (*cf.* Fig. 2a and 3). This result stays in line with the previously reported 2–4 fold increase in the pure optical dephasing time upon temperature drop from 290 K down to 110 K.[37] However, we note that our determined annihilation coherence times are considerably shorter than the corresponding optical dephasing times, indicating that our determined timescale of coherent annihilation represents a lower bound for the electronic coherence timescale. Indeed, in our simplified formulation of the time-dependence of the annihilation constant (eqn (8)) the switch from the coherent regime to the diffusion-limited one occurs instantaneously. Therefore, we do not account for the intermediate process when some coherent excitons still exist but time-dependent annihilation starts to dominate. This simplification eventually

results in shorter coherence times, although the correlation between them and optical dephasing times remains.

The relaxation time of the $E_{22} \rightarrow E_{11}$ transition was found to be about k_{21}^{-1} = 65 fs in all the samples of both single- and double-walled CNTs, again in line with previous studies.[38] Nevertheless, this time, resembling the duration of the laser pulses used, might also be slightly overestimated so that $E_{22} \rightarrow E_{11}$ relaxation may be somewhat faster. The obtained rate of singlet–singlet annihilation was rather slow, $\gamma_0^{-1} \approx$ 3.5–4 ps, and the maximum number of the excitons that can be generated in each manifold was determined to be between 30 and 40 (see Table 1). The latter values are of the same order of magnitude as the saturation exciton density of ~100 excitons per μm evaluated in earlier studies[32] (our CNTs were about 800 nm long).

The most unexpected outcome of our modeling is that in all the cases we examined in this work, the branching parameter α eventually converged to 0. This result holds for the (6,5) tubes embedded in different environments and even for the inner (7,5) tube of the double-walled CNT species, which might indicate the fundamental properties of excitation relaxation pathways common for CNTs of various chiralities. This finding means that after exciton–exciton annihilation the generated doubly-excited $E_{nn} \cong 2E_{11}$ state decays directly into the E_{11} state, bypassing the intermediate E_{22} manifold, as indicated in Fig. 1b. As a result, under E_{11} pumping conditions the E_{22} state remains unpopulated. On the other hand, in the case of the direct E_{22} pump, this state decays with a rate constant $k_{21} = (65\ \text{fs})^{-1}$, so that after a time delay of ~300–400 fs all the excitation should reside in the E_{11} state and exhibit absolutely the same decay behavior as in the case of the E_{11} pump. This effect has been indeed observed and is illustrated in the inset of Fig. 2a, where the excitation kinetics following the E_{22} pump after shifting it to the left by 350 fs overlaps totally with the E_{11} pump kinetics, thus supporting our conclusion that α = 0. Obviously, such a determination of exciton relaxation pathways became possible only by investigating excitation decay kinetics following multiple pumping conditions[12] and was overlooked in the previous studies dealing with just a single case of E_{11} pump.[11,25,26] These results can have serious implications for the impact ionization observed in the CNT photodiodes only upon excitation with the energies exceeding E_{22}.[2] Indeed, excitation to the E_{11} band just induces strong exciton–exciton annihilation, while excitation to higher manifolds can also populate the other available states, those of separated charges in particular. On the other hand, our measurements did not reveal the physical reason for such direct relaxation of doubly-excited excitons bypassing the E_{22} manifold, so that additional experimental studies should be designed to resolve this question. In fact, our obtained result might indicate that some additional intermediate short-lived state is populated followed by a fast relaxation to the E_{11} manifold. Similarly, some additional states could, in principle even participate in the $E_{22} \rightarrow E_{11}$ transition, so that our obtained rates γ_0 and k_{21} might intrinsically account for the relaxation from these states. Nevertheless, we did not introduce these additional possibly existing states in our model since such complication would hardly improve an already good description of the excitation decay kinetics while introducing additional ambiguity to the simulation results due to the increased number of the model parameters.

In this work, we have assumed that the measured transient absorption kinetics, probed at the first optically allowed state E_{11}, follow the dynamics of the ground state bleaching. However, this assumption might not be valid for different probe wavelengths. Indeed, previous studies revealed essential differences between the kinetics probed in (8,3) single-walled CNTs at the E_{11} and E_{22} transitions after E_{11} excitation:[25,26] both kinetics manifested an excellent match between the normalized profile of the kinetics probed at E_{22} transition and the squared profile of the kinetics recorded at the E_{11} wavelength. At the first glance, that observation counteracts our statements of α = 0 since, if E_{22} remains unoccupied, both transient absorption signals probed at E_{11} and E_{22} wavelengths should represent the same kinetics of the $n_1(t)$ population. However, one should note that, despite being very fast, the dynamics of the doubly-excited state E_{nn} can also have some influence. Since under E_{11} pump conditions the E_{22} state remains unpopulated, the detected transient absorption signal can be rewritten, according to eqn (7), as

$$\Delta\text{OD}(t,\lambda) \propto c_1(\lambda)\cdot n_1(t) + c_n(\lambda)\cdot n_n(t),$$

where the weighting factor $c_i(\lambda) = \sigma_i^{\text{ESA}}(\lambda) - \sigma_i^{\text{SE}}(\lambda) - \sigma_0(\lambda)$. When probing at the E_{11} transition, the coefficients c_1 and c_2 are expected to be of the same order, while the E_{nn} population remains almost negligible: $n_n(t) \ll n_1(t)$, so that the detected signal is $\Delta\text{OD}(t, E_{11}) \propto n_1(t)$, as we have used in our simulations. However, when the probe wavelength is set to the E_{22} transition, the cross-section for transitions from E_{nn}, c_n, might become larger than c_1 at the same wavelength. If so, then the observed result is fully consistent with our analysis. This is because from eqn (4) we see that the steady-state population of the E_{nn} manifold is $n_n \propto n_1^2$, so that in this case we obtain $\Delta\text{OD}(t, E_{22}) \propto n_n(t) \propto n_1^2(t)$, *i.e.*

$$\Delta\text{OD}(t,E_{22}) \propto [\Delta\text{OD}(t,E_{11})]^2, \quad (9)$$

the same result that was observed experimentally.[25,26] This effect, obtained for (8,3) CNT species, provides indirect support for our proposal that α = 0 (resulting in excitation relaxation which bypasses the E_{22} manifold entirely) will also hold in other semiconducting CNTs.

A similar relationship between the kinetics probed at the E_{11} and E_{22} manifolds is also observed in the case of the E_{22} pumping conditions, although now the kinetics probed at the E_{22} transition matches the squared profile of the kinetics probed at E_{11} wavelength only asymptotically, after ~0.5 ps following initial excitation (see Fig. 5a). This can be easily understood since at such delay times the population of the E_{22} state completely decays, whereas the remaining populations of the E_{11} and E_{nn} states yield the relationship of eqn (9). For further quantitative verification, we used the population kinetics $n_1(t)$

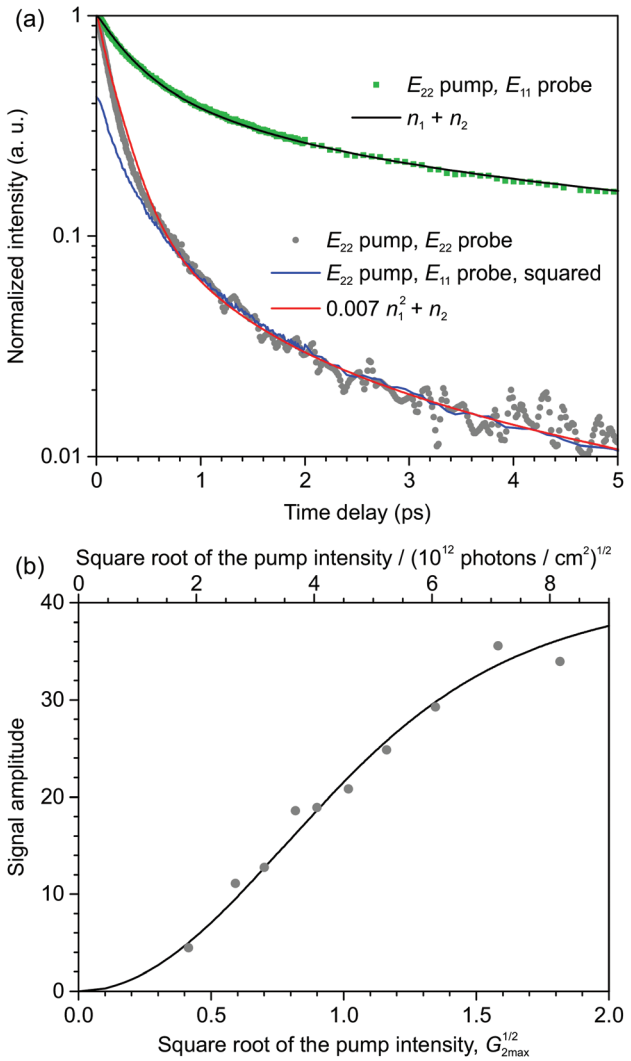

Fig. 5 (a) Comparison of the excitation decay kinetics, probed at the E_{11} and E_{22} transitions following E_{22} excitation. Both the experimental and the fitted kinetics corresponding to the case of the E_{22} pump, E_{11} probe (green squares and black line) are taken from Fig. 2a, the magenta line represents the same kinetics after being squared and rescaled to asymptotically match the E_{22} pump, E_{22} probe kinetics (gray circles). The red line was calculated using the same population kinetics $n_1(t)$ and $n_2(t)$ as obtained from the previous fit using the model parameters listed in Table 1. (b) Dependence of the calculated maximal E_{22}-probed signal, $(0.007{n_1}^2(t) + n_2(t))_{max}$ (see the text), on the excitation intensity G_{2max}, obtained for different pumping conditions using the parameters from Table 1. For comparison, the corresponding experimental observations are also shown with dots by mapping the actually used excitation laser intensities (top axis) to the modeled values of G_{2max}.

and $n_2(t)$, determined from our previous fit in Fig. 2a, to reconstruct the E_{22}-probed kinetics, found to decay as follows: $\Delta OD(t, E_{22}) \propto 0.007{n_1}^2(t) + n_2(t)$ (see red line in Fig. 5). Using the same relationship, we were also able to quantitatively describe the approximately linear dependence of the measured signal amplitude on the square root from the pumping intensity (Fig. 5b). Note that in contrast, the signal probed at the E_{11} transition scales linearly with the G_2 pumping intensity itself and not its square root.[12]

In order to describe low-temperature excitation dynamics in CNTs embedded into a polymer film, we had to introduce an additional energy level E_x in the vicinity of E_{22} manifold. With respect to excitation dynamics, this state acts as a trap that at first enhances the decay of the n_2 population, but eventually re-populates the E_{22} state. From the ratio of the obtained 'trapping' and 'de-trapping' rates, k_{2x} and k_{x2}, we can evaluate the energy difference $\Delta E = E_{22} - E_x \approx 33$ meV, which is much smaller than the exciton binding energy or the energy gap between the E_{11} and E_{22} transitions. As was already mentioned above, the origin of this additional energy state might either be related to the polymer environment or it may represent an intrinsic optically-dark exciton state of the CNTs.[28,33] In the latter case, the same state should in principle also be accounted for when modeling excitation dynamics at room temperature. However, under such conditions, the energy gap ΔE is very similar to the thermal energy k_BT of the lattice phonons, so that both rates k_{2x} and k_{x2} are of the same order and therefore do not influence the overall excitation dynamics very much. This is, however, not the case for double-walled CNTs, for which we had to implicitly include this state in order to properly fit the excitation decay kinetics even at room temperature. Now, the energy gap $E_{22} - E_x$ is about 120 meV which may indicate the effect of inter-tube interactions resulting in the efficient (140 fs, see Table 1) excitation energy transfer from the inner to the outer tube.

6 Concluding remarks

In this work we combined two regimes of exciton–exciton annihilation in carbon nanotubes—the annihilation of coherently delocalized excitons, generated during the initial excitation, and the diffusion-limited regime that starts shortly after the end of the excitation pulse and describes incoherent annihilation of excitons, diffusing along the CNT. The application of this model to the two-color transient absorption measurements of differently prepared samples of single- and double-walled CNTs resulted in a reasonably good description of excitation decay kinetics following both E_{11} and E_{22} pump conditions in the full experimentally accessible time range, from several fs to 15 ps. Simultaneous analysis of both pumping conditions helped us to investigate the possible exciton relaxation pathways. It was shown that after non-linear annihilation a doubly-excited exciton relaxes directly to its E_{11} state bypassing the intermediate E_{22} manifold, so that after excitation, resonant with the E_{11} transition, the E_{22} state remains unpopulated. To complete a self-consistent model of this non-trivial exciton relaxation scheme, we were able to quantitatively explain the much faster excitation kinetics probed at the E_{22} transition compared with the E_{11} probe conditions. In addition, we detected the existence of an additional long-lived optically dark state which is energetically located just slightly below the E_{22} manifold and influences the

dynamics of its population. We believe that these results provide insight into the peculiarities of energy levels and interstate transitions as well as broaden the current understanding of the ultrafast exciton dynamics in semiconducting CNTs.

Acknowledgements

This research was partly supported by EP7 (Marie Curie) project PITN-GA-2012-316633 (POCAONTAS). The work at UC Berkeley was supported by NSF grants CHE-1012168 and CHE-1362830. We also acknowledge the Alex Green and Mark Hersam group of Northwestern for supplying the (6,5) enriched carbon nanotubes, and the Hisanori Shinohara group of Nagoya University for the double-walled carbon nanotube samples used in this work.

References

1 X. Wang, Q. Li, J. Xie, Z. Jin, J. Wang, Y. Li, K. Jiang and S. Fan, *Nano Lett.*, 2009, **9**, 3137–3141.
2 N. M. Gabor, Z. Zhong, K. Bosnick, J. Park and P. L. McEuen, *Science*, 2009, **325**, 1367–1371.
3 A. D. Franklin, M. Luisier, S.-J. Han, G. Tulevski, C. M. Breslin, L. Gignac, M. S. Lundstrom and W. Haensch, *Nano Lett.*, 2012, **12**, 758–762.
4 M. M. Shulaker, G. Hills, N. Patil, H. Wei, H.-Y. Chen, H.-S. P. Wong and S. Mitra, *Nature*, 2013, **501**, 526–530.
5 F. Wang, G. Dukovic, L. E. Brus and T. F. Heinz, *Science*, 2005, **308**, 838–841.
6 Y.-Z. Ma, L. Valkunas, S. M. Bachilo and G. R. Fleming, *J. Phys. Chem. B*, 2005, **109**, 15671–15674.
7 C. D. Spataru, S. Ismail-Beigi, L. X. Benedict and S. G. Louie, *Appl. Phys. A: Solid Surf.*, 2004, **78**, 1129–1136.
8 C. D. Spataru, S. Ismail-Beigi, L. X. Benedict and S. G. Louie, *Phys. Rev. Lett.*, 2004, **92**, 077402.
9 J. Maultzsch, *Phys. Rev. B: Condens. Matter*, 2005, **72**, 241402(R).
10 M. S. Dresselhaus, G. Dresselhaus, R. Saito and A. Jorio, *Annu. Rev. Phys. Chem.*, 2007, **58**, 719–747.
11 L. Lüer, S. Hoseinkhani, D. Polli, J. Crochet, T. Hertel and G. Lanzani, *Nat. Phys.*, 2009, **5**, 54–58.
12 M. W. Graham, J. Chmeliov, Y.-Z. Ma, H. Shinohara, A. A. Green, M. C. Hersam, L. Valkunas and G. R. Fleming, *J. Phys. Chem. B*, 2011, **115**, 5201–5211.
13 T. Koyama, S. Yoshimitsu, Y. Miyata, H. Shinohara, H. Kishida and A. Nakamura, *J. Phys. Chem. C*, 2013, **117**, 20289–20299.
14 M. C. Beard, J. L. Blackburn and M. J. Heben, *Nano Lett.*, 2008, **8**, 4238–4242.
15 S. A. Jensen, R. Ulbricht, A. Narita, X. Feng, K. Müllen, T. Hertel, D. Turchinovich and M. Bonn, *Nano Lett.*, 2013, **13**, 5925–5930.
16 Y. Kumamoto, M. Yoshida, A. Ishii, A. Yokoyama, T. Shimada and Y. K. Kato, *Phys. Rev. Lett.*, 2014, **112**, 117401.
17 G. Soavi, F. Scotognella, D. Viola, T. Hefner, T. Hertel, G. Cerullo and G. Lanzani, *Sci. Rep.*, 2015, **5**, 9681.
18 O. A. Dyatlova, C. Köhler, E. Malic, J. Gomis-Bresco, J. Maultzsch, A. Tsagan-Mandzhiev, T. Watermann, A. Knorr and U. Woggon, *Nano Lett.*, 2012, **12**, 2249–2253.
19 S. M. Santos, B. Yuma, S. Berciaud, J. Shaver, M. Gallart, P. Gilliot, L. Cognet and B. Lounis, *Phys. Rev. Lett.*, 2011, **107**, 187401.
20 B. Yuma, S. Berciaud, J. Besbas, J. Shaver, S. Santos, S. Ghosh, R. B. Weisman, L. Cognet, M. Gallart, M. Ziegler, B. Hönerlage, B. Lounis and P. Gilliot, *Phys. Rev. B: Condens. Matter*, 2013, **87**, 205412.
21 G. Soavi, F. Scotognella, D. Brida, T. Hefner, F. Späth, M. R. Antognazza, T. Hertel, G. Lanzani and G. Cerullo, *J. Phys. Chem. C*, 2013, **117**, 10849–10855.
22 D. Stich, F. Spath, H. Kraus, A. Sperlich, V. Dyakonov and T. Hertel, *Nat. Photonics*, 2014, **8**, 139–144.
23 R. M. Russo, E. J. Mele, C. L. Kane, I. V. Rubtsov, M. J. Therien and D. E. Luzzi, *Phys. Rev. B: Condens. Matter*, 2006, **74**, 041405.
24 Z. Zhu, J. Crochet, M. S. Arnold, M. C. Hersam, H. Ulbricht, D. Resasco and T. Hertel, *J. Phys. Chem. C*, 2007, **111**, 3831–3835.
25 L. Valkunas, Y.-Z. Ma and G. R. Fleming, *Phys. Rev. B: Condens. Matter*, 2006, **73**, 115432.
26 Y.-Z. Ma, L. Valkunas, S. L. Dexheimer, S. M. Bachilo and G. R. Fleming, *Phys. Rev. Lett.*, 2005, **94**, 157402.
27 A. V. Barzykin and M. Tachiya, *Phys. Rev. B: Condens. Matter*, 2005, **72**, 075425.
28 E. B. Barros, R. B. Capaz, A. Jorio, G. G. Samsonidze, A. G. Souza Filho, S. Ismail-Beigi, C. D. Spataru, S. G. Louie, G. Dresselhaus and M. S. Dresselhaus, *Phys. Rev. B: Condens. Matter*, 2006, **73**, 241406.
29 D. M. Harrah, J. R. Schneck, A. A. Green, M. C. Hersam, L. D. Ziegler and A. K. Swan, *ACS Nano*, 2011, **5**, 9898–9906.
30 M. S. Arnold, A. A. Green, J. F. Hulvat, S. I. Stupp and M. C. Hersam, *Nat. Nanotechnol.*, 2006, **1**, 60–65.
31 N. Kishi, S. Kikuchi, P. Ramesh, T. Sugai, Y. Watanabe and H. Shinohara, *J. Phys. Chem. B*, 2006, **110**, 24816–24821.
32 Y. Miyauchi, H. Hirori, K. Matsuda and Y. Kanemitsu, *Phys. Rev. B: Condens. Matter*, 2009, **80**, 081410(R).
33 Y.-Z. Ma, C. D. Spataru, L. Valkunas, S. G. Louie and G. R. Fleming, *Phys. Rev. B: Condens. Matter*, 2006, **74**, 085402.
34 S. Berciaud, L. Cognet and B. Lounis, *Phys. Rev. Lett.*, 2008, **101**, 077402.
35 M. W. Graham, Y.-Z. Ma and G. R. Fleming, *Nano Lett.*, 2008, **8**, 3936–3941.
36 M. Hirtschulz, E. Malic, F. Milde and A. Knorr, *Phys. Rev. B: Condens. Matter*, 2009, **80**, 085405.
37 M. W. Graham, Y.-Z. Ma, A. A. Green, M. C. Hersam and G. R. Fleming, *J. Chem. Phys.*, 2011, **134**, 034504.
38 C. Manzoni, A. Gambetta, E. Menna, M. Meneghetti, G. Lanzani and G. Cerullo, *Phys. Rev. Lett.*, 2005, **94**, 207401.

